Time-Resolved Molecular Frame Dynamics of Fixed-in-Space CS_2 Molecules.

Christer Z. Bisgaard,[1] Owen J. Clarkin,[1,2] Guorong Wu,[1]
Anthony M. D. Lee,[1,2,†] Oliver Geßner,[3] Carl C. Hayden,[4] Albert Stolow[1,2*]

[1]Steacie Institute for Molecular Sciences, National Research Council Canada,
100 Sussex Drive, Ottawa, ON K1A 0R6, Canada
[2]Department of Chemistry, Queen's University,
Kingston, ON K7L 3N6, Canada
[3]Chemical Sciences Division, Lawrence Berkeley National Laboratory,
One Cyclotron Road, M/S 2-300, Berkeley, CA 94720, USA
[4]Combustion Research Facility, Sandia National Laboratory, Livermore, CA 94551, USA

[†]Present address: Department of Cancer Imaging, BC Cancer Research Centre,
Vancouver BC V5Z 1L3, Canada
[*]To whom correspondence should be addressed; E-mail: albert.stolow@nrc.ca.

Laser-induced alignment is used to transiently fix a molecule in space long enough to study its dynamics in the molecular frame, elucidating ultrafast chemical processes.

Random orientation of molecules within a sample leads to blurred observations of chemical reactions studied from the laboratory perspective. Methods developed for the dynamic imaging of molecular structures and processes struggle with this, as measurements are optimally made in the molecular frame. Here we use laser alignment to transiently fix CS_2 molecules in space long enough to elucidate, in the molecular reference frame, details of ultrafast electronic-vibrational dynamics during a photochemical reaction. These three-dimensional

photoelectron imaging results, combined with ongoing efforts in molecular alignment and orientation, presage a wide range of insights obtainable from time-resolved studies in the molecular frame.

Most molecules are non-spherical and so exhibit a dependence on their relative orientation in interactions with other molecules or with light. Measurements, therefore, should ideally be made in the molecular reference frame (MF). Unfortunately, in the gas and liquid phases, molecules are generally randomly oriented in the laboratory frame (LF) to which most standard techniques are referenced, leading to blurred observations of molecular properties and processes. An analogy is the difference between single crystal versus powder X-ray diffraction, the former revealing the greatest details of molecular structure. Other examples include the determination of vector-correlations in photodissociation dynamics (*1*) and measurements of (time-independent) photoelectron angular distributions (PADs) of fixed-in-space molecules which has been a goal of researchers since the 1970s (*2*) and was achieved for selected cases (*3,4*). Promising ultrafast techniques for imaging structural and electronic changes during molecular processes, such as time-resolved X-ray (*5*) and electron (*6,7*) diffraction, tomographic orbital imaging (*8*), time-resolved photoelectron spectroscopy (*9,10*), laser-induced electron diffraction (*11*) and high harmonic generation (*12*), would all benefit from avoidance of this orientational averaging of MF observables. Here we present ultrafast time-resolved imaging measurements of a complex molecular process – a nonadiabatic photochemical reaction – from the MF, employing a laser technique which transiently fixes the molecules' alignment in space for sufficiently long to permit field-free dynamic measurements.

Strong non-resonant laser fields can induce molecular axes alignment within the LF (*13*), but may themselves modify excited state dynamics (*14*). The goal of probing molecules which are aligned but field-free can be accomplished by applying a short laser pulse (*15*) that leaves the molecules transiently aligned (i.e. fixed-in-space) for, typically, a few picoseconds. This very

brief molecular alignment can only be fully exploited by ultrafast measurement techniques, in our case by time-resolved photoelectron spectroscopy (TRPES), a method sensitive to both electronic and vibrational rearrangements (*16–19*). We chose to investigate the non-adiabatic photodissociation reaction $CS_2 + h\nu \rightarrow CS_2^* \rightarrow$ CS(X) + S(^{1}D) / S(^{3}P). CS_2 is notable as a triatomic system because it exhibits three general features of photodissociation dynamics: vibrational mode coupling, internal conversion and intersystem crossing. Consequently, CS_2 has complex photodissociation dynamics and, despite numerous studies, many details remain unresolved (*20*). Our study of coupled electronic and vibrational rearrangements occurring during this reaction combined impulsive alignment (*15*) with time-resolved photoelectron 3D imaging (*10*) and quantum beat spectroscopy (*21*) to reveal details of the scattering resonances discernable only within the MF.

The ultraviolet (UV, 200 nm) photodynamics of the initially linear CS_2 molecule involves complex non-adiabatic and spin-orbit mixing, leading to multiple product states. The excitation from a non-bonding S-atom orbital to an anti-bonding π^* molecular orbital lengthens the C-S bonds and leads to a bent equilibrium geometry. Thus, the absorption spectrum contains progressions assigned to combined excitations of the symmetric stretch and bend vibrations. In addition, nonadiabatic interactions with a nearby excited state leads to the mixing of electronic character at bent geometries. The excited state bending frequency is nearly degenerate with that of the considerably weakened symmetric stretch, leading to combination bands of symmetric stretch and bend with peaks spaced by $\sim$400 cm^{-1}, each further split ($\sim$30 cm^{-1}) due to this near degeneracy (*22*). The barrier to linearity in this electronically excited state is around 49600 cm^{-1} (201.6 nm), the excitation energy used in our experiments. Franck-Condon factors therefore favor excitation into a quasi-linear geometry. Since photoabsorption leads to dissociation, these spectral peaks may be understood as photodissociation scattering resonances having lifetimes exceeding several vibrational periods. The two open product channels, CS +

S(^3P_J) and CS + S($^1D_2$), have a wavelength dependent branching ratio (*23*) and broad translational energy distributions (*24*). From the peak widths in the absorption and S-atom action spectra, resonance lifetimes of less than 1 ps were estimated (*23*). Femtosecond time-resolved ion yield (*25,26*) and photoelectron (*20*) measurements confirmed this sub-picosecond behavior. Coexisting with the sharp resonances in the 6 eV region is a broad underlying continuum (*23*) due to very short-lived scattering resonances (direct dissociation) involving the anti-symmetric stretch vibration (*27*).

A depiction of our time-resolved photoelectron probing of CS_2 photodissociation dynamics is presented in Fig. 1. Following transient alignment of the CS_2 a fs UV pump pulse prepared a coherent superposition of scattering resonances in a linear geometry, leading to quasi-bound vibrational motions followed by dissociation to both singlet and triplet products (Fig. 1). This superposition was probed as a function of time by delayed a probe pulse (125 fs pump-probe cross-correlation) which ionized the molecule. The emitted photoelectron was analyzed as a function of energy, 3D recoil angle, and pump-probe delay. Importantly, the duration of the alignment ($\sim$4 ps FWHM) was longer than the time scale of the photoreaction ($<$ 1 ps), rendering the molecules effectively fixed-in-space during the measurement.

The resolved series of resonances allowed us to combine our time-resolved photoelectron 3D imaging method (*28*) with another powerful technique for probing excited state dynamics: quantum beat spectroscopy (*21*). By tuning the central wavelength (bandwidth $\sim$ 250 cm^{-1}) of our fs pump laser to 201.2 nm, we coherently prepared a superposition of two scattering resonances, differing only in the degree of symmetric stretch vs. bending excitation. Quantum interference in photoionization of coherently prepared scattering resonances was previously reported in ion yield measurements for IBr (*29*) and CS_2 (*26*) photodissociation. In the present case, the quantum beat interference between two long-lived scattering resonances in our MF photoelectron data permits access to intimate details of the electronic-vibrational couplings

associated with the decay of these resonances.

A time-resolved photoelectron spectrum acquired for unaligned CS_2 is given in Fig. 2(a), showing photoelectron kinetic energies as a function of delay. The 0.7 eV peak at short delays, broadened due to an unresolved 55 meV spin-orbit splitting, arises from ionization into the vibrationless (0,0,0) cation ground state. The low energy features correspond to ionization into highly excited vibrational states. The time-resolved spectrum is composed of: a fast initial decay as well as a slow decay across the whole spectrum, and a slow, periodic modulation of the high-energy electrons. We employed 2D global methods to simultaneously fit all photoelectron energies at all time delays to within experimental errors. Our kinetic model involved two independent exponential decays, with the longer one modulated by a harmonic oscillation (*28*). The global fit yielded time-constants of $\tau_1 = 70 \pm 20$ fs, and $\tau_2 = 830 \pm 40$ fs with a modulation period of $T = 1010 \pm 20$ fs. The decay-associated photoelectron spectra of these three kinetic components are presented in Fig. 2(b). As expected, the long lived τ_2 component samples highly distorted geometries that ionize to vibrationally excited ions (low photoelectron energies). In Fig. 2(c) we show the time evolution of the LF photoelectron signal at 0.7 eV and the global fit (red line), corresponding to ionization into the cation (0,0,0) ground state. The quantum beat signal can be clearly seen. The extracted time constant τ_2 is in very good agreement with the lifetime estimated from analysis of rotational band contours in the action spectrum (*23*). The 1010 fs period matches the 34 cm^{-1} splitting observed at 201 nm in the absorption spectrum. We can therefore assign the periodic modulation to the quantum beat interference between the two quasi-bound scattering resonances. Our measurements confirm both the previously reported quantum beat (*26*) and the bi-exponential decay (*20*) measurements. The time constant τ_1 confirms the presence of broad, short-lived resonances (*23*). The laser alignment of CS_2 leaves these global time constants unchanged (i.e. the fitted MF and LF time constants are the same), suggesting that ground state vibrations are not excited by the alignment laser.

This kinetic model of CS_2 excited state decay reveals insuffient details of the underlying electronic-vibrational dynamics of the resonance decay. To advance, we applied the transient alignment method to make MF measurements. In Figure 3 we show the two-photon ion yield as a function of the delay between the alignment pulse and the 201 nm pump pulse, in the vicinity of the rotational half-revival (greatest alignment). To quantify the alignment, we carried out simulations taking into account thermal averaging, spatial focal volume averaging over laser intensities, and the relative magnitudes of the parallel vs. perpendicular ionization transition dipoles (*28*). The red curve in Fig. 3 shows the best fit to a degree of alignment of $\langle \cos^2 \theta \rangle = 0.55 \pm 0.03$. Within the pump-probe window (<1.5 ps) across which MF time-resolved measurements were carried out, the molecules were effectively fixed-in-space.

To acquire time-resolved MF PADs of CS_2 photodissociation, we set the delay between the alignment and pump pulses to 73.5 ps, slightly before the maximal alignment. The 201 nm fs pump pulse, polarized parallel to the alignment axis, interacted with this aligned sample. Due to the parallel transition dipole, excitation further sharpened the excited state alignment to an estimated value $\langle \cos^2 \theta \rangle = 0.74$. Energy-resolved PADs resulting from photoionization due to the 268 nm fs probe laser, also polarized parallel to the alignment axis, were recorded as a function of pump-probe delay within the time window shown in Fig. 3. The MF PADs for ionization into the (0,0,0) state of the cation (Fig. 2(c)) are shown at five time delays on the right side of Fig. 4. The analogous PADs for the unaligned sample are given on the left. A dramatic change in the MF PADs is observed in the photoelectron intensity parallel to the MF axis. At early times there is a local minimum along the MF direction, whereas at t=500 fs there is a maximum in this direction. At t=900 fs, the MF PAD has mostly reverted back to its form at t=100 fs. As confirmed by the time scale, this is due to the quantum beat interference in the MF PAD between the two scattering resonances.

The selection of the MF PADs in Figure 4 from the (0,0,0) cation ground state has important

implications for the analysis of their structure and time evolution. First, Franck-Condon (FC) factors restrict photoionization to quasi-linear geometries, simplifying a symmetry analysis. Second, photoionization of either scattering resonance produced the same cation vibrational state. Within the Born-Oppenheimer and FC approximations, electronic and nuclear dynamics are fully separated and both resonances should produce the same PADs (i.e. the free electron departs from the same ion core), differing only in amplitude due to their distinct FC factors. If the PAD shape also varies during the quantum beat, as in Fig. 4, then the PADs from the two scattering resonances must differ in form. This means that there must be a vibrational coordinate dependence to the ionization transition dipole - a failure of the FC approximation.

This coordinate dependence can originate from the variation of electronic structure with vibrational coordinates in the final continuum state, the neutral excited state, or both. Our final state is the (0,0,0) state of the strongly bound cation: the vibrational wave function is restricted to a small range of internuclear distances where we do not expect mixing with other cation electronic states. We also argue that there are no resonances in the ionization continuum within our range of energies (see Supporting Text). Therefore, neither the cation nor the free electron wave function likely has strong vibrational coordinate dependence. It is rather the nuclear coordinate dependence of the electronic character of the excited neutral state which causes the PADs to evolve during the quantum beat, and signifies the differential electronic character sampled by the different vibrational excursions of the two scattering resonances.

This explanation is strongly supported by theory. In our case, one scattering resonance has more symmetric stretch character and less bend amplitude whereas the other has the opposite. Energetically located just above the linear initial state ($^1\Sigma_u^+$) is an optically dark state ($^1\Pi_g$). In linear geometries, these two states do not interact. Upon bending, however, the degenerate upper state splits into two components, one of which interacts strongly with the initial state upon bending and stretching. Therefore, as shown in the inset of Fig. 1, we expect mixing of Π_g

character into the wavefunction as the molecule bends and stretches (q). We thus attribute the time evolution of the MF PADs in Fig. 4 to the difference in bending and stretching amplitude between the two scattering resonances, sampling different degrees of Π_g character upon vibration. Our calculations reveal a strong mixing between these states at very small bending angles (Fig. S2 and Supporting Text).

A complete determination of the photoionization dynamics requires knowledge of the amplitudes and phases for all partial waves. While approximate methods for determining photoionization amplitudes exist, calculating the phase shifts of all partial waves for excited states of a polyatomic molecule undergoing non-adiabatic dynamics is currently computationally intractable. Furthermore, attempts to extract amplitudes and phases directly from the data will not yield a unique fit to the PADs. Therefore, precluding a detailed analysis of the photoionization dynamics, we consider a symmetry analysis based on the quasi-linear behavior sampled by our (0,0,0) final state (*28*). The quantum beat phenomenon leads to signals which oscillate between the sum and the difference of the two ionization transitions. Therefore, the PADs at t=100 fs and t=900 fs reflect the average electronic character of the two scattering resonances, whereas the PAD at t=500 fs reflects the difference in electronic characters between the two. The symmetry-expected MF PAD from the initial state (t=100 fs) has minima in directions both parallel and perpendicular to the molecular axis. As seen from Fig. 4, this expectation is in good qualitative agreement (consistent with imperfect axis alignment) with the MF PAD observed at t=100 fs. By t=500 fs (corresponding to the minimum of the quantum beat in Fig. 2(c)) the angular distribution appears qualitatively different, now peaking parallel to the MF axis. The PAD observed at t=500 fs is consistent with ionization from a state of Π_g symmetry, the expected difference between the two resonance wavefunctions. By t=900 fs, approaching the first maximum of the quantum beat, the MF PADs appears again very similar to that at t=100 fs.

Simplifying still further, if we employ single-active electron pictures, the MF PADs are di-

rectly determined by the initial orbital and the MF direction of the ionization transition dipole (*19, 28*). The changes in the PADs then directly reflect changes in orbital character. In the FC region, the initial state is predominantly of $n \rightarrow \pi^*$ character (the corresponding orbital is plotted at the top-right of Fig. 4). As the molecule bends and stretches, state mixing introduces some $n \rightarrow \sigma^*$ character (middle-right of Fig. 4). The qualitative changes in the MF PADs agree well with the changes in orbital character of the excited state, as the quantum beat phenomenon amplifies the differences between the two resonances. The MF PADs do show an energy dependence (Fig. S1): different ion vibrational states exhibit different PADs. However, their temporal evolution is very similar to that of the (0,0,0) state, with comparable changes at all energies. That the PADs are final state dependent is consistent with the different ion states having different Condon points and therefore reflecting different aspects of the excited state evolution.

The fact that the MF PADs exhibit an oscillatory behavior which is in phase at all energies highlights an important aspect of this observable (*16*): the time evolution of the PADs (Fig. 4) for fixed-in-space molecules is predominantly determined by changes in the electronic symmetry of the excited state. By contrast, the time evolution of the photoelectron spectrum (Fig. 2) is primarily sensitive to the vibrational dynamics and population decay: when several vibrational states of the cation are accessible, details of the dynamics may become obscured by averaging over these states. This is why the quantum beat is not observed in the photoelectron yield at low electron energies but stands out clearly in the MF PADs. In a simple model, the PADs are determined by the shape of the orbital being ionized and the ionic potential from which the electron is ejected. For small amplitude vibrational motion, which is ensured by our choice of final state, the changes in the PADs are then mostly determined by the re-organization of the electrons due to the coupling between electronic states. The time-evolution of the photoelectron spectrum and the MF PADs therefore add complementary information about the dynamics, highlighting the

power of combining field-free alignment techniques with ultrafast spectroscopy.

References and Notes

1. T. P. Rakitzis, A. J. van den Brom, M. H. M. Janssen, *Science* **303**, 1852 (2004).

2. D. Dill, *J. Chem. Phys.* **65**, 1130 (1976).

3. J. H. D. Eland, *J. Chem. Phys.* **70**, 2926 (1979).

4. K. G. Low, P. D. Hampton, I. Powis, *Chem. Phys.* **100**, 401 (1985).

5. A. M. Lindenberg, *et al.*, *Science* **308**, 392 (2005).

6. H. Ihee, *et al.*, *Science* **291**, 458 (2001).

7. B. J. Siwick, J. R. Dwyer, R. E. Jordan, R. J. D. Miller, *Science* **302**, 1382 (2003).

8. J. Itatani, *et al.*, *Nature* **432**, 867 (2004).

9. V. Blanchet, M. Z. Zgierski, T. Seideman, A. Stolow, *Nature (London)* **401**, 52 (1999).

10. O. Geßner, *et al.*, *Science* **311**, 219 (2006).

11. M. Meckel, *et al.*, *Science* **320**, 1478 (2008).

12. W. Li, *et al.*, *Science* **322**, 1207 (2008).

13. H. Stapelfeldt, T. Seidemann, *Rev. Mod. Phys.* **75**, 543 (2003).

14. B. J. Sussman, D. Townsend, M. Y. Ivanov, A. Stolow, *Science* **314**, 278 (2006).

15. F. Rosca-Pruna, M. J. J. Vrakking, *Phys. Rev. Lett.* **87**, 153902 (2001).

16. T. Seideman, *Annu. Rev. Phys. Chem.* **53**, 41 (2002).

17. K. L. Reid, *Annu. Rev. Phys. Chem.* **54**, 397 (2003).

18. T. Suzuki, *Ann. Rev. Phys. Chem.* **57**, 555 (2006).

19. A. Stolow, J. G. Underwood, *Adv. Chem. Phys.* **139**, 497 (2008).

20. D. Townsend, *et al.*, *J. Chem. Phys.* **125**, 234302 (2006).

21. E. Hack, J. R. Huber, *Int. Rev. Phys. Chem.* **10**, 287 (1991).

22. R. J. Hemley, D. G. Leopold, J. L. Roebber, V. Vaida, *J. Chem. Phys.* **79**, 5219 (1983).

23. A. Mank, C. Starrs, M. N. Jego, J. W. Hepburn, *J. Chem. Phys.* **104**, 3609 (1996).

24. D. Xu, J. Huang, W. M. Jackson, *J. Chem. Phys.* **120**, 3051 (2004).

25. A. P. Baronavski, J. C. Owrutsky, *Chem. Phys. Lett.* **221**, 419 (1994).

26. P. Farmanara, V. Stert, W. Radloff, *J. Chem. Phys.* **111**, 5338 (1999).

27. R. R. Sadeghi, S. R. Gwaltney, J. L. Krause, R. T. Skodje, P. M. Weber, *J. Chem. Phys.* **107**, 6570 (1997).

28. Materials and methods are available as supporting material on *Science* Online.

29. M. J. J. Vrakking, D. M. Villeneuve, A. Stolow, *J. Chem. Phys.* **105**, 5647 (1996).

30. Supported by the Natural Sciences and Engineering Research Council of Canada (A.M.D.L. and A.S.). We gratefully acknowledge Jonathan Underwood, Serguei Patchkovskii, Cheuk-Yiu Ng, Mark Brouard and David M. Wardlaw for stimulating discussions. This work was supported by the Director, Office of Science, Office of Basic Energy Sciences, Chemical Sciences Division of the U.S. Department of Energy under Contract No. DE-AC02-05CH11231 (O.G.).

Figure 1: Schematic representation of our femtosecond time-resolved photoelectron 3D imaging measurements of the pre-dissociation dynamics of CS_2. Dissociation proceeds via asymmetric stretching to singlet and triplet products. Due to the geometry change in the excited state, the initial nuclear motion proceeds along the bending and symmetric stretch coordinates (blue trajectory). Upon bending and stretching, the excited Σ_u^+ state adiabatically develops Π_g electronic character (inset). The quasi-bound dynamics are probed by measuring the energy and 3D emission direction of the photoelectrons emitted upon ionization into the bound ground state of the cation.

Figure 2: (a) The time-resolved photoelectron spectrum of CS_2 following excitation to the $^1\Sigma_u^+$ state pumped at 201.2 nm. The decay-associated spectra resulting from a 2D global analysis of the data are shown in (b), with the photoelectron signal fit at all energies and all delays simultaneously. In (c) we show the evolution of the photoelectron band corresponding to ionization into the vibrational ground state of the cation, along with the result of the global fit. The quantum beat can be clearly seen.

Figure 3: Jet-cooled CS_2 molecules are transiently aligned by a short (100 fs), non-resonant (805 nm) laser pulse, creating a rotational wavepacket. The alignment dynamics around the half-revival are monitored via the two-photon ionization yield (blue dots). To estimate the degree of alignment, we simulated the ion-yield as a function of delay using direct integration of the time-dependent Schrödinger equation to propagate the rotational wavepacket. The calculated axis angular distribution is shown in the inset for the ground state (blue) and excited state (red) molecules. Within the window used for the pump-probe experiment (red band), the molecules are fixed-in-space.

Figure 4: Time-resolved PADs for unaligned (left) and aligned (right) CS_2 molecules. The LF laser polarization vectors are shown at top right. Also shown are the orbitals with the highest contribution to the state evolving adiabatically from the $^1B_2(^1\Sigma_u^+)$ state in the Franck-Condon

region. Top and bottom right panels show the π^* orbital that dominates in the Franck-Condon region, whereas the middle right panel shows the σ^* orbital that contributes at geometries that are both stretched and bent. The MF PADs (aligned) reveal details of the dynamics not seen in the randomly aligned sample.

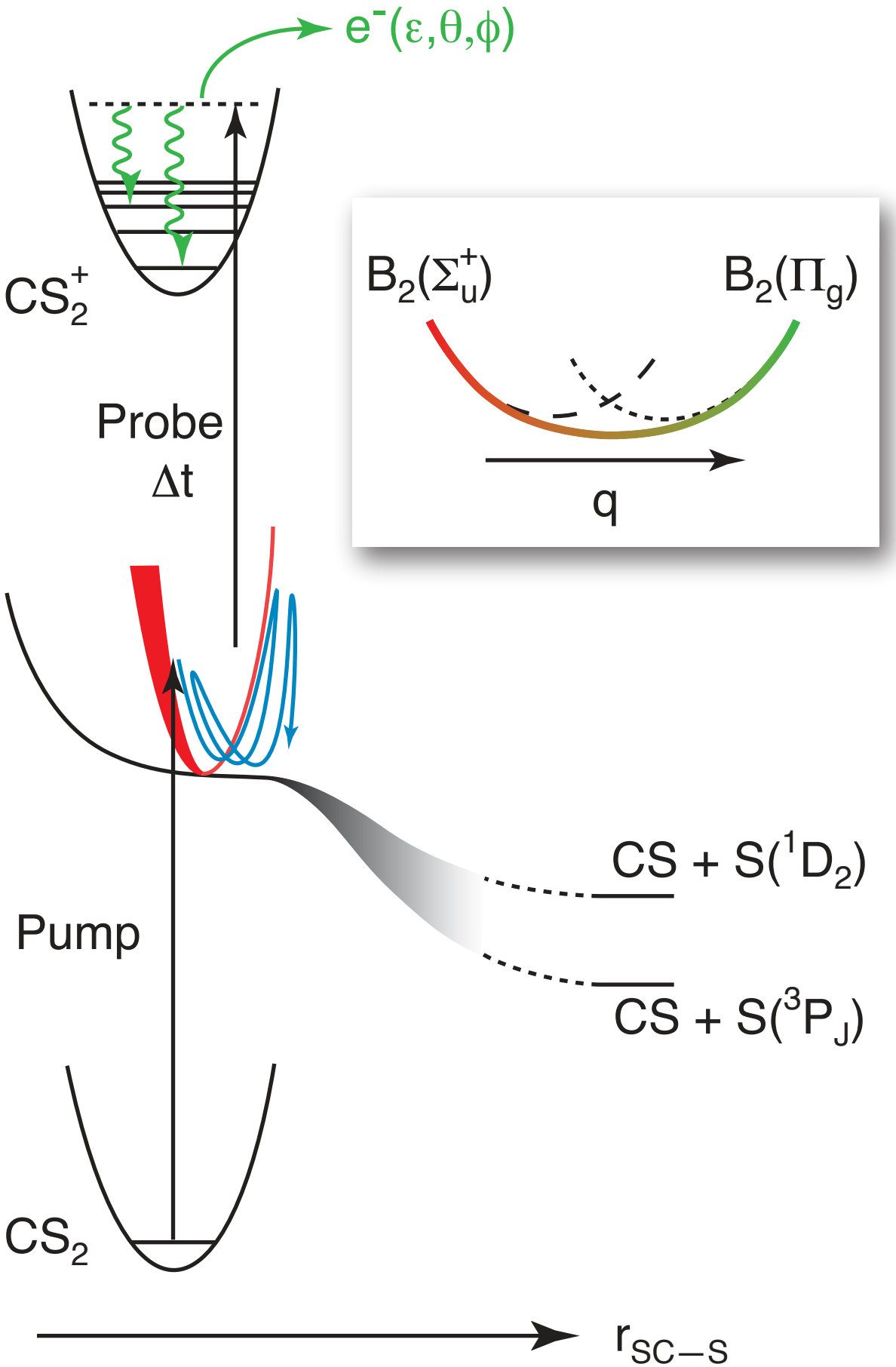

Fig. 1

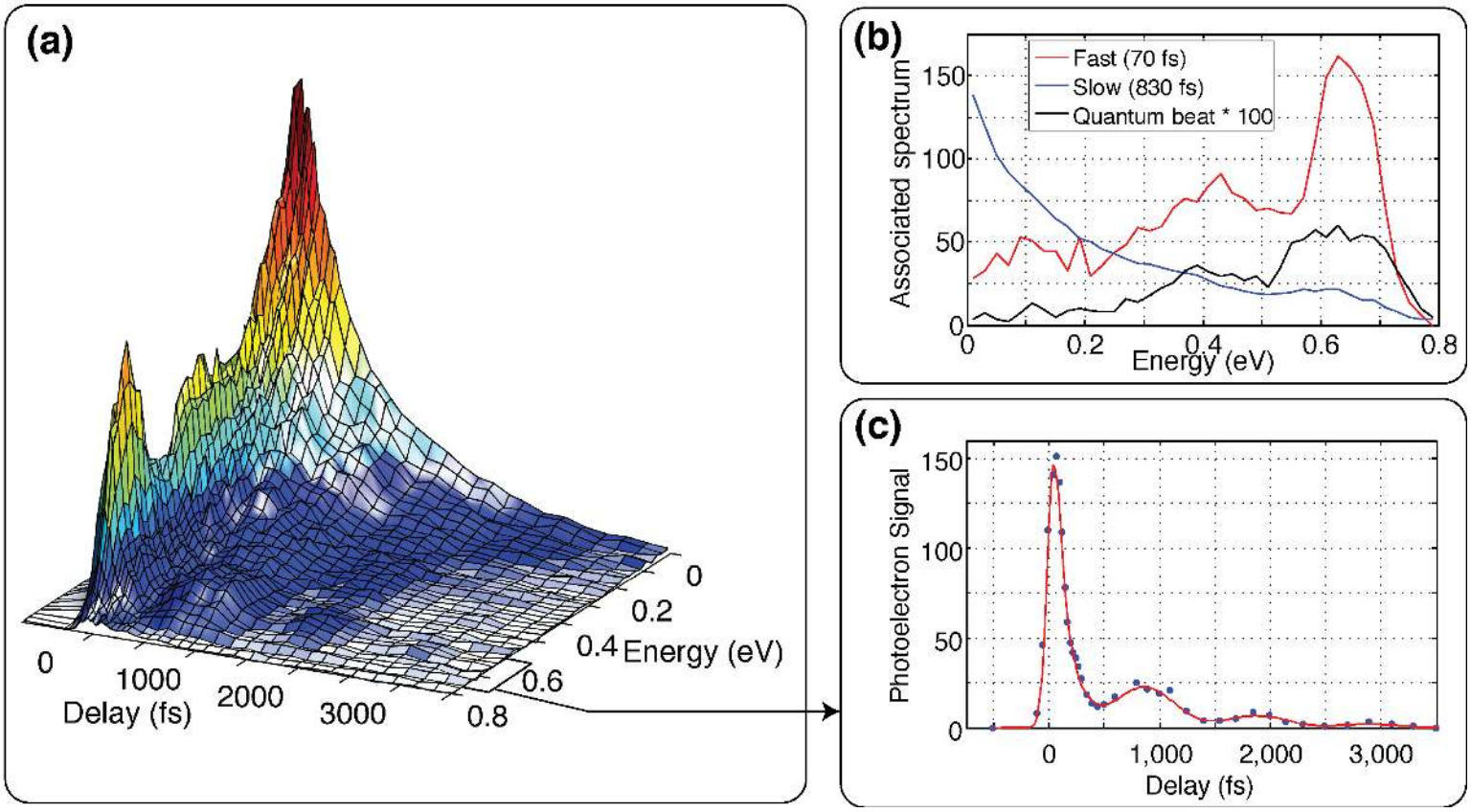
(a)
0
1000
2000
3000
Delay (fs)
0
0.2
0.4
0.6
0.8
Energy (eV)
(b)
Fast (70 fs)
Slow (830 fs)
Quantum beat * 100
Associated spectrum
150
100
50
0
0
0.2
0.4
0.6
0.8
Energy (eV)
(c)
Photoelectron Signal
150
100
50
0
0
1,000
2,000
3,000
Delay (fs)

Fig. 2

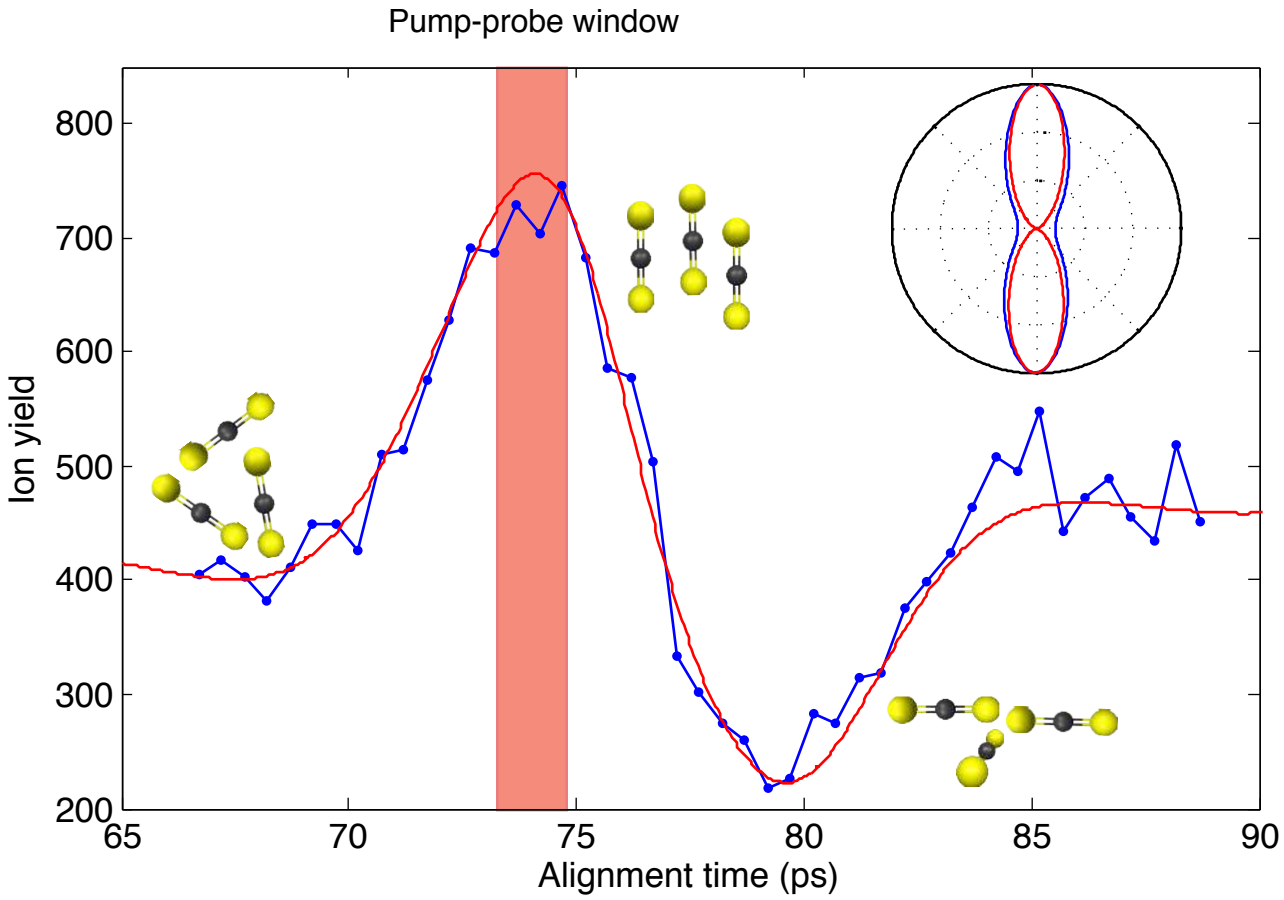
Pump-probe window
Ion yield
800
700
600
500
400
300
200
65
70
75
80
85
90
Alignment time (ps)

Fig. 3

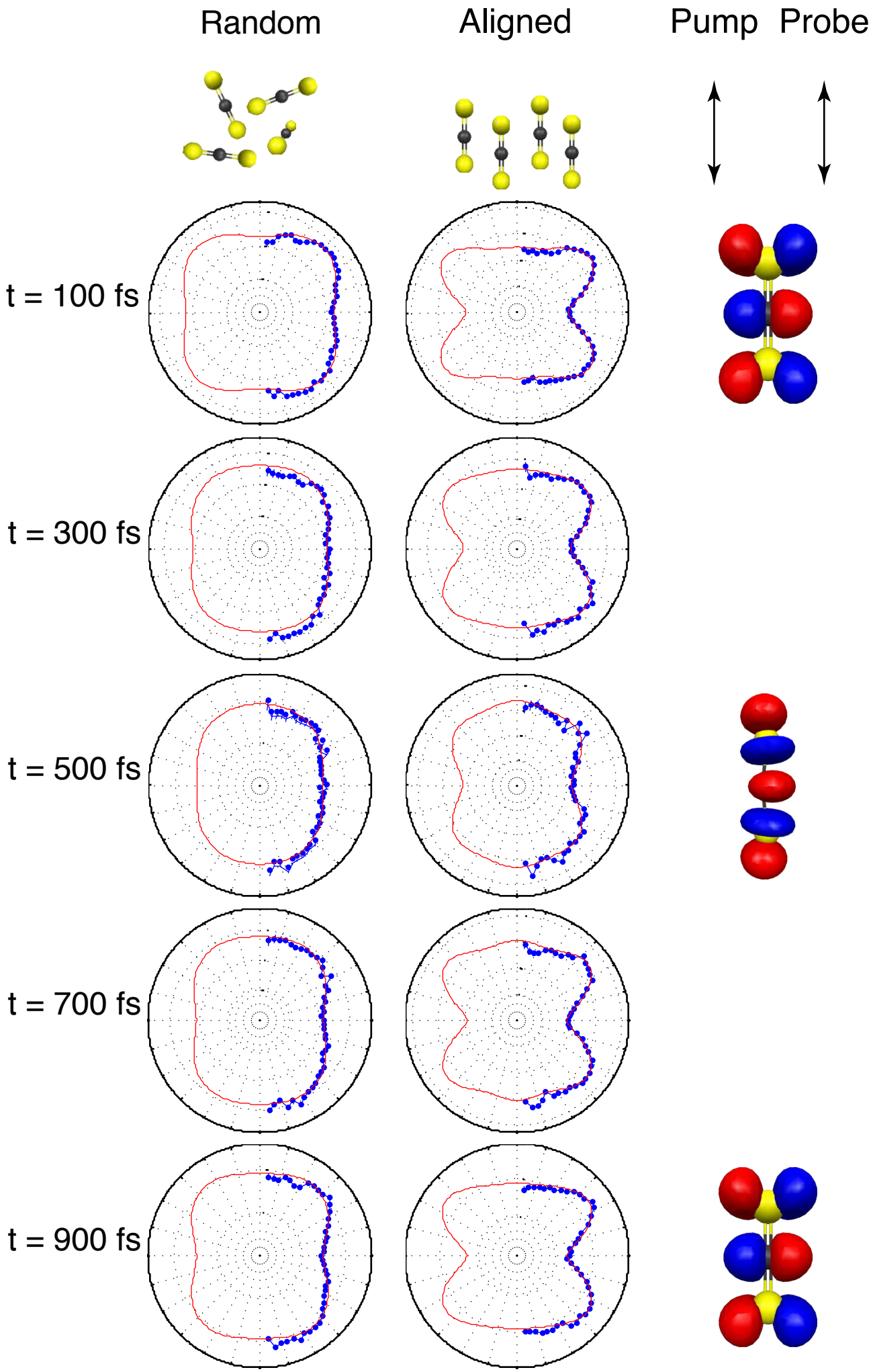
Random
Aligned
Pump
Probe
t = 100 fs
t = 300 fs
t = 500 fs
t = 700 fs
t = 900 fs

Fig. 4